THE PENNSYLVANIA STATE UNIVERSITY
SCHREYER HONORS COLLEGE

DEPARTMENT OF CHEMICAL ENGINEERING

EFFECT OF SURFACTANT CONCENTRATION ON ALUMINA NANOPARTICLE-NICKEL-IRON COMPOSITES

OWEN T. REINERT
SPRING 2018

A thesis
submitted in partial fulfillment
of the requirements
for a baccalaureate degree
in Chemical Engineering
with honors in Chemical Engineering

Reviewed and approved* by the following:

Manish Kumar
Associate Professor of Chemical Engineering
Thesis Supervisor

Andrew Zydney
Distinguished Professor of Chemical Engineering
Honors Adviser

* Signatures are on file in the Schreyer Honors College.

ABSTRACT

Iron and nickel alloys serve as catalysts in several industries despite their quick degradation. Previous research has shown that addition of alumina nanoparticles can affect corrosion and catalytic properties, but no research has investigated the effects of nanoparticle dispersion on these properties. The parameter of nanoparticle dispersion was varied by varying the amount of surfactant in the solution used for electrodeposition. The objective of this thesis was to evaluate various testing techniques to determine their efficacy for nano-scale surfaces while calculating corrosion parameters such as polarization resistance and corrosion current, as a function of surfactant concentration. Experiments were performed by sequentially increasing the surfactant concentration before electrodeposition, with the resulting samples subjected to various characterizations and corrosion tests. Investigative techniques included scanning electron microscopy and energy dispersive X-ray spectroscopy (SEM-EDX), X-ray diffraction (XRD), galvanodynamic scanning (GDS), linear polarization resistance (LPR), electrochemical impedance spectroscopy (EIS), and electrochemical frequency modulation (EFM. It was found that most corrosion properties followed a checkmark or inverted checkmark pattern, with the 1 g/L and the 100 g/L samples being the extrema. The Tafel constant decreases and corrosion voltage increases in excess of 1 g/L surfactant. This indicates that when corrosion is slowest (1 g/L SDS) it also is thermodynamically the most likely to occur. The 100 g/L SDS sample was quickest but least thermodynamically likely to corrode, potentially indicating a passivation layer. XRD was found to be ineffective for very thin films. EFM proved to be better at calculating the Tafel constant because EFM directly yields the Tafel constant, while GDS requires guesswork when slopes are not precisely linear.

TABLE OF CONTENTS

LIST OF FIGURES

LIST OF TABLES

ACKNOWLEDGEMENTS

I would like to thank Dr. Michael Janik and Dr. Manish Kumar for helping me obtain this research position. Thanks to Dr. Shannon Servoss and Jesse Roberts for helping me excel in my research. Additionally, thanks to Dr. Lauren Greenlee, Sergio Iván Pérez Bakovic, Prashant Acharya and Mojtaba Abolhassani for their guidance on my specific project. I would also like to thank Dr. Andrew Zydney for advising, proofreading, and advocating on my behalf. Finally, I would like to thank my family for their endless support and love; none of my accomplishments would have come to fruition without them.

This research was funded by National Science Foundation REU Grant # EEC-1659653.

Chapter 1

Problem Statement

An important property that can be changed via electrodeposition is the catalytic behavior of the material, which is especially pertinent to fuel cell technologies. Electrodeposition of nickel and iron alloys onto a working electrode of carbon nanotubes has already been shown to increase electrocatalytic activity in air-hydrazine fuel cells (Wang et al., 2013), and to be potentially useful for the oxygen evolution reaction (OER) in a hydrogen fuel cell (Kim et al., 2012). These materials are of particular interest because they are not noble metals, allowing for much cheaper production and better scalability.

Catalysts degrade over time, and these iron and nickel based catalysts are no exception. Iron helps the alloy be more reactive, but this also means it degrades more quickly. This relationship is because most corrosion occurs as a reaction on the catalyst surface, much like the desired reaction. Therefore, by studying corrosion properties, insight about the catalytic properties is also gained. This degradation typically occurs via iron dissolving into solution, going from neutral to either the Fe^{2+} or Fe^{3+} species. If more electrons were readily available on the catalyst, the longevity of these catalysts could be improved.

With the emergence of nanosurface engineering, various techniques for characterization and corrosion testing used in traditional experiments may not be effective at that scale. Common techniques for characterization of electrodeposited films include scanning electron microscopy and energy dispersive x-ray spectroscopy (SEM-EDX), x-ray diffraction (XRD) and inductively coupled plasma mass spectrometry (ICP-MS). Corrosion resistance can be determined by

conducting electrochemical frequency modulation (EFM), electrochemical impedance spectroscopy (EIS), linear polarization resistance (LPR) and galvanodynamic scanning (GDS). These techniques need to be evaluated at the nanoscale in order to inform researchers which tests they should conduct on their thin films for characterization and determination of corrosive properties.

The objective for this thesis is to conduct an evaluation of various common experiments, pertaining to both characterization and corrosion, using an investigation of how surfactant concentration affects these properties as the exigence.

Chapter 2

Background and Hypothesis

Electrodeposition is the process of applying a current or potential via electrodes to a metallic salt solution, called a bath, in order to reduce some of the salts to solids on the cathode. This process is essentially a galvanic cell operating in reverse, where the goal is not to generate power, but to form a layer over the working electrode, also known as the cathode. The circuit is completed by an anode, which is called the counter electrode. This layer is typically either for decorative purposes, like a copper coating on US pennies (US Mint: Coin Production, 2017), or for enhancing certain properties, such as a coating of nickel to increase corrosion resistance (Nickel Plating Handbook, 2014).

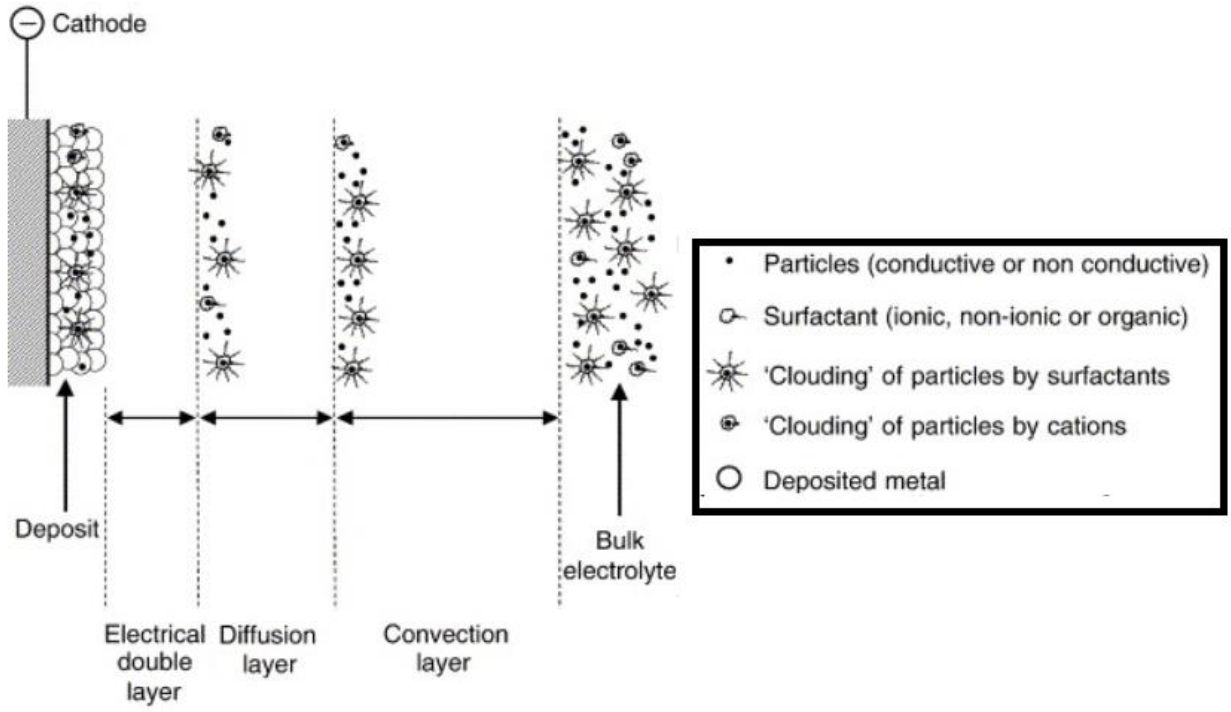

Figure 1. Layers in the electrodeposition process (Roos et al., 1990).

Within the bath, various layers are defined by their proximity to the working electrode. In order to be deposited, metal ions must move from the bulk electrolyte to the electrode by passing through the convection layer, diffusion layer, and electrical double layer in that order. Material flow is controlled by bulk movement in the convection layer, but becomes dependent on diffusive processes in the diffusion layer. The diffusion layer is typically on the order of hundreds of micrometers, and is due to the presence of a concentration boundary layer. The electrical double layer is caused by a significant change in electric potential near the working electrode, and serves as the final resistance to adsorption. A depiction of these various layers can be seen in Figure 1 above.

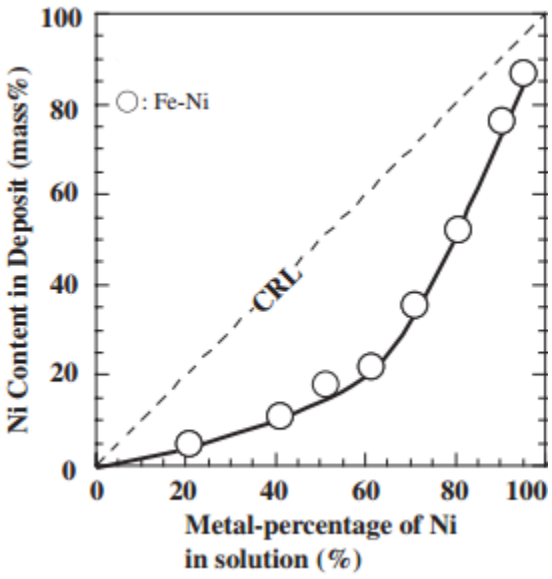

Figure 2. Nickel deposition as a function of bath composition (Nakano et al., 2004).

Iron and nickel electrodepositions are run simultaneously to create an alloy, and this process is called codeposition. The relative percentages of each metal making up the alloy does not vary linearly with the bath percentages; under most conditions, nickel will make up a

significantly lower percentage of the alloy than what was present in the solution (Nakano et al., 2004). This can be seen in Figure 2. Nickel is more noble than iron, so nickel should normally have a higher affinity to return to a neutral state via adsorption; the deposition is called anomalous because this is not what is observed. This is thought to be partially because iron forms iron hydroxides before depositing that inhibit the deposition of nickel. Using chloride salts has been shown to reduce this inhibition and decrease the overpotential. Overpotential is the difference between the potential expected from the half reactions in the cell, and the potential observed. It is essentially a measure of voltage efficiency, where a lower overpotential is more efficient. Research has also suggested that iron is diffusion limited during this process, and that the stirring speed of the solution has a significant impact on the iron composition of the alloy (Torabinejad et al., 2017). The stirring speed helps decrease the diffusion resistance to the surface and its effect can be seen in Figure 3.

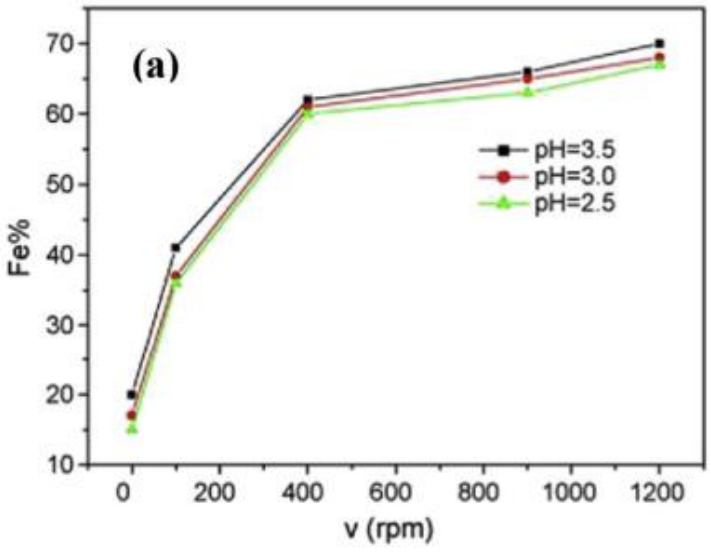

Figure 3. Iron composition is dependent on stirring speed (Torabinejad et al., 2017)

The application of alumina nanoparticles to slow down corrosion in similar systems has already been demonstrated (Starosta et al., 2004). Alumina nanoparticles act as a sacrificial oxidant on the surface; when iron is oxidized to Fe^{2+} or Fe^{1+}, the alumina will reduce the iron back to neutral. This will continue to work until alumina has no more electrons to give, at which point the system should corrode as if there were no alumina nanoparticles present.

Many advantages of electrodepositing multiple components, some of them being non-metallic, have already been researched (Williams, 1966). Several additives such as citric acid (Ghorbani et al., 2002), boric acid (Wu et al., 2003) and saccharin (Bhandari et al., 2009) have been shown to affect how deposition occurs. Additionally, surfactants are additives that play a critical role in preventing nanoparticle aggregation (Vadivel et al., 2015). Surfactants are typically compounds that contain a polar head, and a long nonpolar tail, such as sodium dodecyl sulfate (SDS). These compounds help nonpolar species better dissolve in polar species by lowering the surface tension experienced at boundaries, such as the surface area of alumina nanoparticles in aqueous solution.

Despite this knowledge, it is unknown how the concentration of surfactant affects surface properties during electrodeposition. By investigating this phenomenon, it could provide another variable for manipulating nickel and iron nanosurfaces. This would be pertinent for not only water treatment applications, but also for water splitting catalysis, pipeline longevity, and ammonia synthesis. Recently, iron and nickel alloys have also been used to convert methane and carbon dioxide into synthesis gas (More et al., 2016). Understanding the effects of surfactants will allow better manipulation of nanosurfaces for the development of new materials.

The overall goal of introducing alumina nanoparticles into nickel and iron surfaces is to achieve higher corrosion resistance or improved catalytic properties. By investigating how

surfactants impact these properties, we hope to identify and characterize an additional method of manipulation for future inquiry. The hypothesis for these experiments is that increasing surfactant concentration increases corrosion resistance due to the greater spacing of the sacrificial oxidizing nanoparticles. Currently, the main parameters being used to change surface properties, and thus create new materials, are based on the electrical specifics, chemical additives, as well as the overall composition of iron and nickel in solution. Surfactants are known to disperse nanoparticles, but the goal of this research is to precisely evaluate how much of this additive should be used in order to control certain properties. Additionally, this research serves to evaluate various testing techniques for their efficacy on thin composite films formed by electrodeposition.

Chapter 3

Materials and Methods

3.1 Preparation and Composition of Electrodeposition Solution

The concentrations of each electrodeposition solution component can be found in Table 1 below. The combination of sulfate and chloride metal salts produces a bath that is more conductive (due to chloride ions) but also supplies ample metal cations (due to sulfate ions). Boric acid serves as a pH stabilizer, while saccharin helps relieve internal stresses in the film. Saccharin deposits sulfur at grain boundaries, reducing the tensile stress at these boundaries (Bhandari et al., 2009). It is a common additive in Ni-Fe alloy baths for this reason. Sodium dodecyl sulfate was added throughout the experiment in order to aid nanoparticle dispersion.

Table 1. Chemical composition of the electrodeposition bath

Chemical	Concentration (g/L)
Nickel Sulfate Hexahydrate	10
Nickel Chloride Hexahydrate	1.6
Iron Sulfate Septahydrate	2
Boric Acid	1.4
Saccharin	0.04
Alumina Nanoparticles	2
Sodium Dodecyl Sulfate	0-100

The bath was prepared by first measuring nickel sulfate hexahydrate, nickel chloride hexahydrate, iron sulfate septahydrate, boric acid, and saccharin and combining these elements in water at approximately 75% of the desired volume. Then, aqueous alumina nanoparticles (20 wt. % in water from Sigma-Aldrich) were added. Water was used to achieve the final desired volume. This mixture was centrifuged for approximately 5 minutes at 1000 rpm to aid in homogenizing the solution. Centrifugation helped break down the salts that were not entirely dissolved because the solution remained lumpy even after mixing. Most experiments were run in approximately 40 mL of solution. The solution was allowed to stir overnight at 500 rpm at 50^{o}C.

3.2 Electrodeposition Procedure

A picture of the electrochemical cell used in each of these depositions can be seen in Figure 4. The stainless steel (SS) working electrode is connected to a red alligator clip, which is connected to the Gamry Potentiostat Reference 3000. The counter electrode consists of two pieces of carbon paper connected via Ag / Cu wire to another alligator clip. The reason for designing the cell to have counter electrode area on both sides of the working electrode is to minimize variability of the plating between each side of the working electrode.

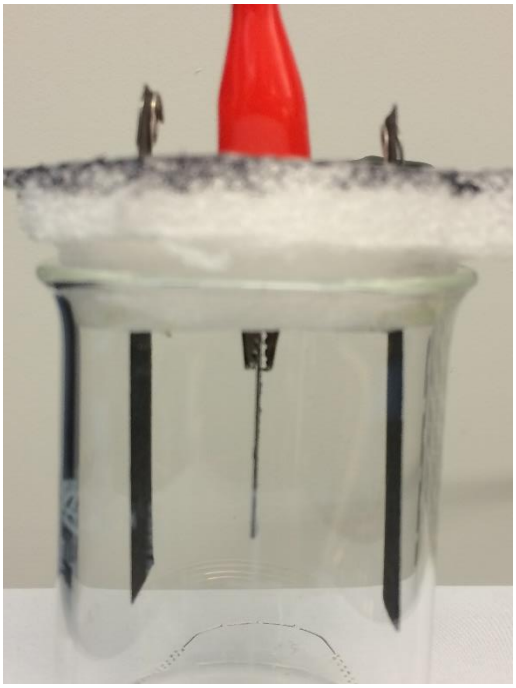

Figure 4. Electrochemical cell used for each electrodeposition

A series of steps were repeated in order to gather all of the required data. First, the solution was sonicated for 30 minutes at approximately 20 – 30 ^{o}C. Then, the solution was added into the electrochemical cell with a stir bar. The cell was placed on top of a dual hot and stir plate; four minutes were given for the solution to thermally equilibrate with the 50^{o}C hot plate with stirring at 100 rpm. The deposition was then run twice, both times for 200 seconds each at a current density of 3 A/dm^2 and a duty cycle of 90%. Duty cycle refers to the time that current is being sent through the circuit divided by the total time elapsed. This pulsation helps negate some of the diffusion resistance, as it allows species that get depleted (iron) to reconcentrate near the surface of the working electrode. The deposition was done by using the cyclic chronopotentiometry experiment in the Gamry Framework software. Sodium dodecyl sulfate was then added to the solution, and it was stirred for another 3 minutes at 500 rpm. These steps were then repeated, starting again with 30 minutes of sonication. This was repeated for SDS concentrations of 0, 0.1, 1, 10 and 100 g/L.

3.3 Characterization Experiments and Procedures

Scanning electron microscopy and energy-dispersive X-ray spectroscopy (SEM-EDX) and X-ray diffraction (XRD) were run in order to characterize the composition and phase of the samples. Inductively coupled plasma – mass spectrometry (ICP-MS) protocols were developed, but the test was not completed. Both SEM-EDX and XRD should be run before ICP-MS because ICP-MS will destroy the sample.

3.3.1 Scanning Electron Microscopy and Energy-Dispersive X-ray Spectroscopy

Scanning electron microscopy allows the various structures on the surface of the film to be observed. Tests were conducted using a FEI XL-30 Environmental Scanning Electron Microscope. This microscope does not require surfaces to be covered with a layer of gold or carbon to increase conductivity; for this reason, it was selected to examine the films in their natural state. Samples were attached to SEM sample pin stubs by using two-sided carbon tape. The film quality could differ slightly on each side of the same working electrode, so the side that appeared to have less uniform or total deposition was used to secure the sample. Pictures were taken as the magnification was increased to a maximum of approximately 350,000x.

Accompanying this visualization technique, energy dispersive X-ray spectroscopy was used to identify the relative amounts of each of the following elements: iron, nickel and aluminum. No additional preparation was required to run EDX on a sample; upon being inserted into the SEM, random locations were sampled and their atomic composition was recorded. The scanning feature was used to correlate visual structures to atomic element.

3.3.2 X-ray Diffraction

A Philips Xpert Powder XRD was used to conduct this test over the range of $40 < 2\theta < 55$. This range was chosen because it includes peaks of various Ni-Fe phases. The side of the working electrode with a larger, uniform coating area was chosen to be exposed to the laser. The sample was held in place with clear tape at the corners, outside of the area of analysis. This test was initially run quickly (total duration of approximately 20 minutes), then refined by using a longer scanning time (total duration of approximately 90 minutes).

3.3.3 Inductively Coupled Plasma – Mass Spectrometry

Even though the actual ICP-MS was not conducted, the developed procedure is of value for future experiments. The film and substrate of choice (SS) shared some of the same elements, viz. nickel. So, the entire working electrode could not be directly submerged into nitric acid to complete the digestion necessary for ICP-MS. To work around this, clear tape was pressed firmly onto the film, and subsequently ripped off. The tape was then placed in a beaker with acetone and sonicated for 20 minutes. Finally, the acetone was decanted, and the beaker was placed in the fume hood; only parts of the metal film remained in the beaker after the rest of the acetone evaporated. This also allowed the weight of the recovered film to be determined.

3.4 Corrosion Experiments and Procedures

All corrosion tests were conducted using the Gamry Potentiostat Reference 3000 in a 3.5 wt% solution of sodium chloride with a silver / silver chloride reference electrode. The counter

electrode was carbon paper of approximately 3-4 times larger area than the working electrode. This helped to reduce diffusive resistance from the counter electrode. Unless otherwise stated, samples were placed in the 3.5 wt% NaCl solution, allowed to equilibrate for 4 minutes, and subsequently tested. Electrochemical impedance spectroscopy should be run first, followed by electrochemical frequency modulation. Both of these corrosion tests are nondestructive because they operate at very slight deviations from open circuit potential (OCP). Electrochemical impedance spectroscopy provides information about the frequency that should be used to conduct electrochemical frequency modulation. Then, electrochemical frequency modulation provides a way to calculate directly the Tafel constant of the working electrode. The Tafel constant is a kinetic parameter that represents the amount of overpotential that must be applied in order to increase the corrosion (reaction) rate by a factor of 10.

3.4.1 Electrochemical Impedance Spectroscopy

Electrochemical impedance spectroscopy (EIS) was able to estimate the polarization resistance (R_p) and non-capacitive frequency region of the sample. Impedance is the equivalent of resistance for alternating current and must be differentiated from resistance because of an additional degree of freedom. Impedance has phase and magnitude, whereas resistance only has magnitude. EIS data can be expressed on a Bode or Nyquist plot. Bode plots yield the non-capacitive frequency region where the slope of the impedance magnitude approaches zero on the left side of the graph (at low frequencies). This region is important to determine because it will help achieve more accurate results when conducting electrochemical frequency modulation. Bode plots have separate curves that display the magnitude and phase of impedance, while the Nyquist

plot consists of one curve that accounts for both components. The Nyquist plot approximates the polarization resistance by modeling where the curve would intersect the X-axis (forming a semi-circle). This can be compared with the results of LPR. A more detailed description of EIS and how to use equivalent electrical circuits to model results can be found in Appendix B.

In addition to determining R_p and the non-capacitive region, EIS also gives an idea of whether or not the corrosion system is diffusion limited. A Nyquist plot appearing as a 45-degree line signifies that semi-infinite diffusion limits the rate. Plots that form a half circle indicate reaction limited electrodeposition. Plots that transition from a quarter circle into a 45-degree line indicate a mixed control system, where some frequencies are diffusion limited and others are reaction limited. These data can be used to determine the validity of other tests, such as galvanodynamic scanning. If the Nyquist plot depicts clear diffusion limitations, then galvanodynamic scanning will not yield accurate Tafel constants.

3.4.2 Electrochemical Frequency Modulation

Electrochemical frequency modulation (EFM) will not work as effectively if there is capacitance in the system. A base frequency of 0.01 Hz with multipliers of 2 and 5 was used. This test has built in causality factors (2 and 3) which serve as internal checks to see if the data are of good quality. Staying in the non-capacitive region (as determined by EIS) helps achieve more accurate causality factors. When operating in the correct frequency range, EFM provides an avenue to calculate directly the Tafel constant via a Fourier transform and harmonic analysis.

3.4.3 Galvanodynamic Scanning

Galvanodynamic scanning (GDS) works by measuring the potential when varying the current. On a semi-log graph of potential versus current, the linear regions of the graph are used to calculate the corrosion potential (E_{corr}) and the corrosion current (I_{corr}). This test also yields the Tafel constant. Some error can be associated with pinpointing the exact end of the linear region of the graph. Linearity is important in order to determine the Tafel constant because these linear regions are reaction limited; the kinetic parameter cannot accurately be measured when diffusion is limiting the rate of corrosion.

3.4.4 Linear Polarization Resistance

Linear polarization resistance (LPR) was conducted by scanning +/- 10 mV around the open circuit potential (OCP). Open circuit potential refers to the electrical potential present when there is no external current or potential applied to the system. The slope of this graph represents the polarization resistance and can be checked against the results of electrochemical impedance spectroscopy. A higher polarization resistance means that it is exceedingly unfavorable for a surface to react. This corresponds to a lower corrosion rate.

Chapter 4

Results and Discussion

4.1 Characterization Experiments

The characterization experiments being investigated are SEM-EDX, XRD, and ICP-MS. The individual results of each test will first be discussed, and then the tests will be compared.

4.1.1 Scanning Electron Microscopy and Energy-Dispersive X-ray Spectroscopy

SEM-EDX yielded a significant amount of information regarding the structures present on the nanometers thick film. EDX was used to determine what various colors corresponded to what elements; a large area scan found below shows that the lighter, white specks correspond to the alumina nanoparticles. The rest of the visible background was made up of iron and nickel of various phases, unable to be determined by this test explicitly. This visual confirmation was confirmed by doing point EDX and noticing a large peak of aluminum on the white specks.

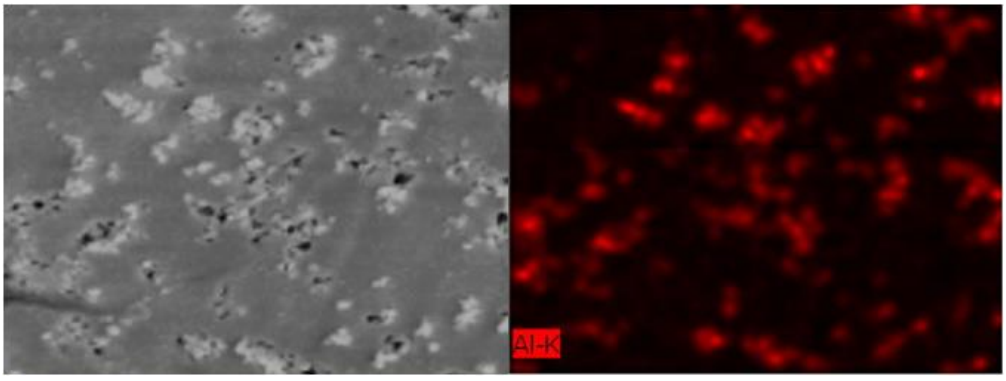

Figure 5. EDX shows white specks on a 1 g/L sample are concentrated in aluminum

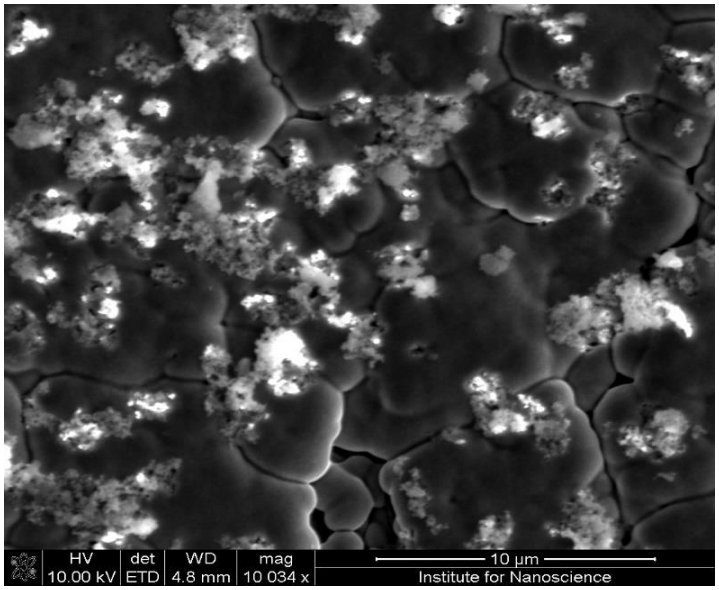

Figure 6. SEM image from a film produced in 0 g/L SDS bath

While the point analysis did confirm that the white specks were likely alumina nanoparticles, it did little to determine the exact composition of the film at large. Individual runs of EDX resulted in vastly different estimated compositions depending on even very slight changes in location. Additionally, some areas showed up to 20 wt% chromium. This means that it was not practical to determine the bulk composition of the film via this method for films produced in any concentration of SDS. However, changes in phases as SDS increased was observed. At low concentrations of SDS, significant nanoparticle aggregation was observed across the surface. A picture taken from a plating done at an SDS concentration of 0 g/L is shown above. As the concentration increased, overall nanoparticle aggregation was not as severe. Additionally, what appears to be holes in the film started to appear and thin nano-crystalline structures can be seen in the background of the film. The holes seem indicative of a changing amount of internal stresses within the film, causing the film to break. These regions are also concentrated by white patches, and an example of this can be seen below.

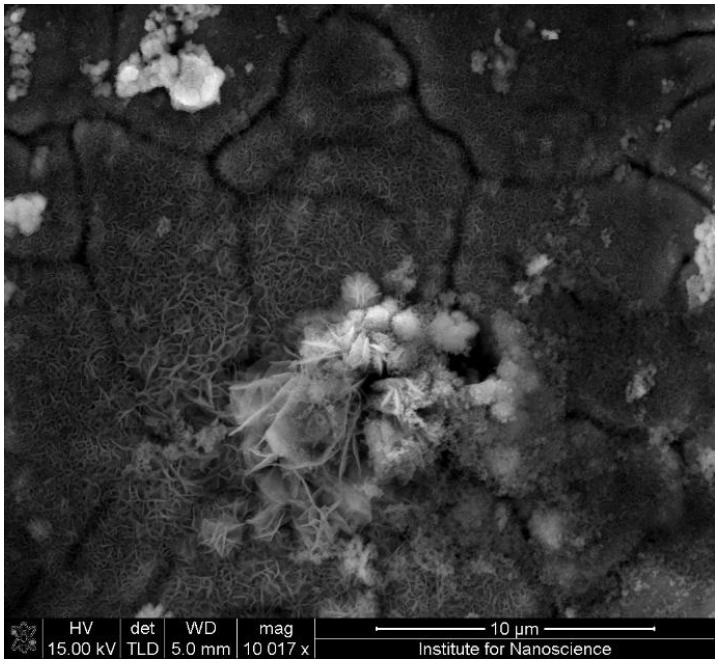

Figure 7. SEM image from a film produced in 10 g/L SDS bath

The image below was taken at 1 g/L. It shows a single nanoparticle embedded on the surface and indicates that despite aggregation occurring at every SDS concentration,not all of the nanoparticles did aggregate.

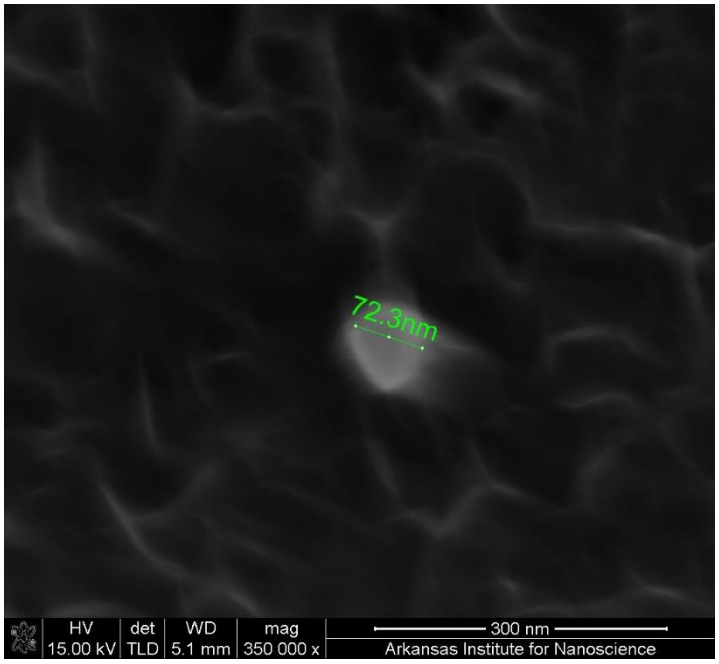

Figure 8. Single nanoparticle from a film produced in 1 g/L SDS bath

4.1.2 X-ray Diffraction

XRD on the thin composite film yielded what appeared to be successful results. However, the peaks matched exactly to the stainless steel used as substrate for the electrodeposition. The test was already conducted at a low power to decrease the average penetration depth of x-rays into the material. However, this corrective measure was still not enough to get a successful reading from XRD. For very thin films, XRD proved unreliable at determining phase or composition. After determining that the results only showed peaks of stainless steel, the experiment was not repeated.

4.1.3 Inductively Coupled Plasma – Mass Spectrometry

While the test was not conducted, the results from the developed procedure were positive. The procedure outlined in Chapter 3.1.3 succeeded in isolating a known weight of each film, and

would have allowed for easy digestion in a nitric acid solution. A disadvantage of this technique was that the entire film was not recoverable, meaning that the true average composition would be impossible to determine. Electrodeposition tends to create less than uniform films, which makes figuring out the exact composition exceedingly difficult.

4.1.4 Summary of Characterization Experiments

XRD was not able to operate on the extremely thin films produced by this series of experiments. SEM-EDX provided valuable information about the topography of each film, and showed different phases of iron and nickel that had developed on the films. It also confirmed the changing aggregation properties of the nanoparticles. The disadvantages of using SEM-EDX are that the technique was unable to determine what exact phases of iron and nickel were present, only that the two phases differed. Additionally, this technique was ineffective at determining the specific composition of the overall film. Therefore, it could not accurately determine properties such as overall weight percentage of each element in the film. ICP-MS involves digestion of the film in acid, and could have been used to determine the overall weight percentage of each element. Additionally, the technique could have determined if the number of alumina nanoparticles varied greatly between films. Despite not running the actual experiment, the protocol developed in order to digest the films proved effective in minimizing the amount of substrate removed with the desired film. This process would help yield more precise results when utilizing ICP-MS because other techniques would allow the nitric acid to dissolve some of the substrate. A procedure of first conducting SEM-EDX and then ICP-MS would likely produce the necessary data for any thin film series. XRD would only prove effective for thicker films.

4.2 Corrosion Experiments

The results of each corrosion experiment will first be individually discussed. The order of this analysis will parallel the order in which the experiments were conducted on samples, with the nondestructive tests (EIS, EFM) first, then the destructive tests later (GDS, LPR).

4.2.1 Electrochemical Impedance Spectroscopy

The table below summarizes the results from EIS. The Gamry dedicated software was able to determine not only the goodness of fit for a CPE model, but also the 95% confidence intervals for the determined values. Goodness of fit is ideally 0, where 0 indicates a perfect fit. The highest deviation from ideality was during the 100 g/L sample experimental run.

Table 2. Polarization and solution resistances with tolerance from EIS

SDS Concentration (g/L)	0	0.1	1	10	100
R_p (ohm-cm^2)	4700±40	3950±40	5000±100	4440±50	8710±80
R_u (ohm-cm^2)	9.94±0.07	10.51±0.08	11.21±0.09	10.53±0.08	11.43±0.08
Goodness of Fit	0.044	0.04	0.034	0.05	0.061

Appendix B breaks down the specifics of how this test was conducted. A simple model with two resistors and one constant phase element was used to fit the data. The trends of calculated R_p and solution resistance (R_u) for each sample can be seen in the figure below. The solution resistance was slightly higher at 100 g/L concentration of SDS, which could also correspond to the notable viscosity difference between the 10 and 100 g/L electrodeposition baths.

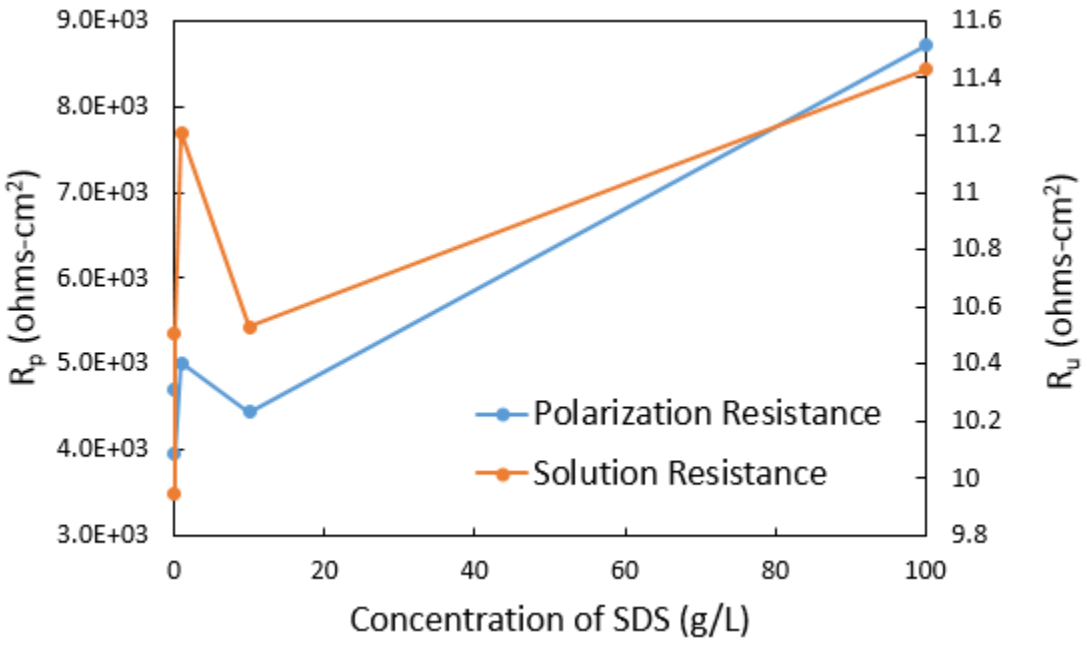

Figure 9. Polarization and solution resistances as a function of SDS concentration

The checkmark shape found for most other tests is not seen above. It is possible that the 1 or 100 g/L data point is erroneous. The data point at 1 g/L SDS appears to be an outlier based on a closer analysis of the data fit. The data on the Nyquist plot only encompasses a half circle. While the model fits the curve well, it has to extrapolate considerably in order to calculate the polarization resistance. Typically, the fit is below the true curve on a Nyquist plot, resulting in a lower estimated R_p. This was not the case, as shown by the figure below. The fact that the Nyquist plot does not appear to trail downwards may indicate the system is under mixed control, and that at some frequencies diffusion takes over the system.

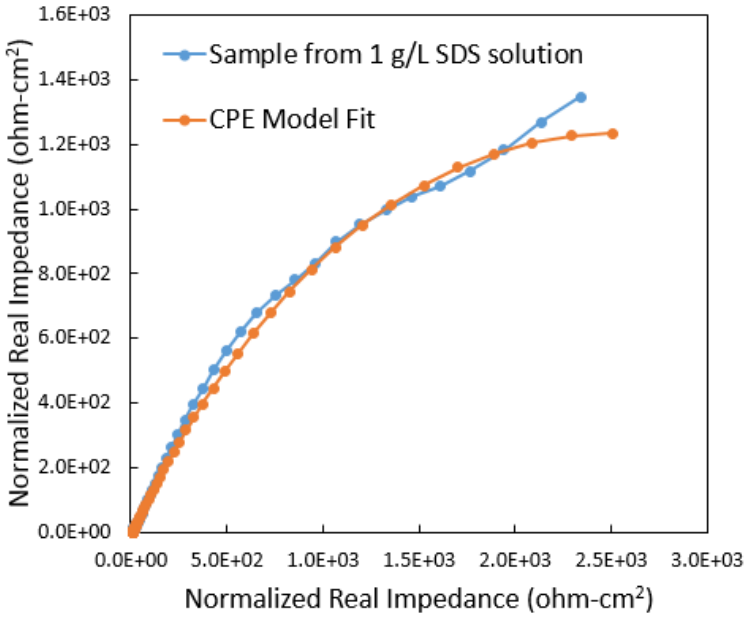

Figure 10. Nyquist plot of kinetically controlled model on 1 g/L SDS sample

The Bode plot also shows that the non-capacitive region is never reached, so a larger frequency region would be required for future tests. This can be seen in the figure below. The non-capacitive region is typically seen at low frequencies and is when the curve displaying the magnitude of impedance flattens out. With the Gamry instrument, these lower frequencies resulted in significantly increased noise. Therefore, instruments that are more precise may be required to achieve accurate data at lower frequencies.

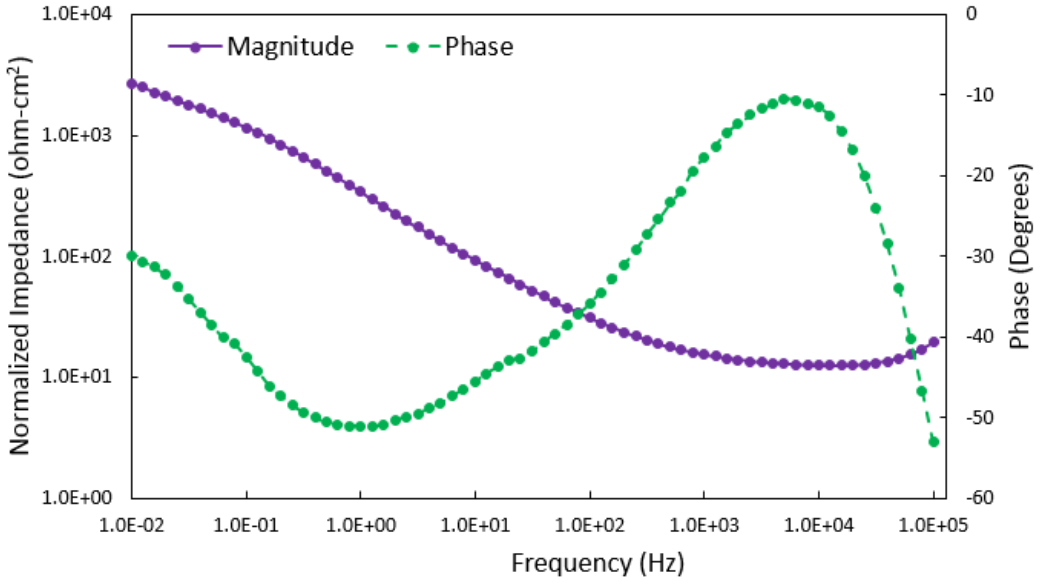

Figure 11. Bode plot of sample produced in 1 g/L SDS

The 100 g/L sample data was also investigated. Upon running Kramers Kronig analysis, the data appear not to be accurate. The large deviation from the Kramers Kronig analysis indicates that excessive noise was present in the system and resulted in problematic data. This deviation can be seen in the figure below. It is possible that too much impedance was already in the system, or that instruments that are more precise are required for EIS to be effective. These observations are consistent with the fact that the 100 g/L sample has the largest goodness of fit value of 0.061.

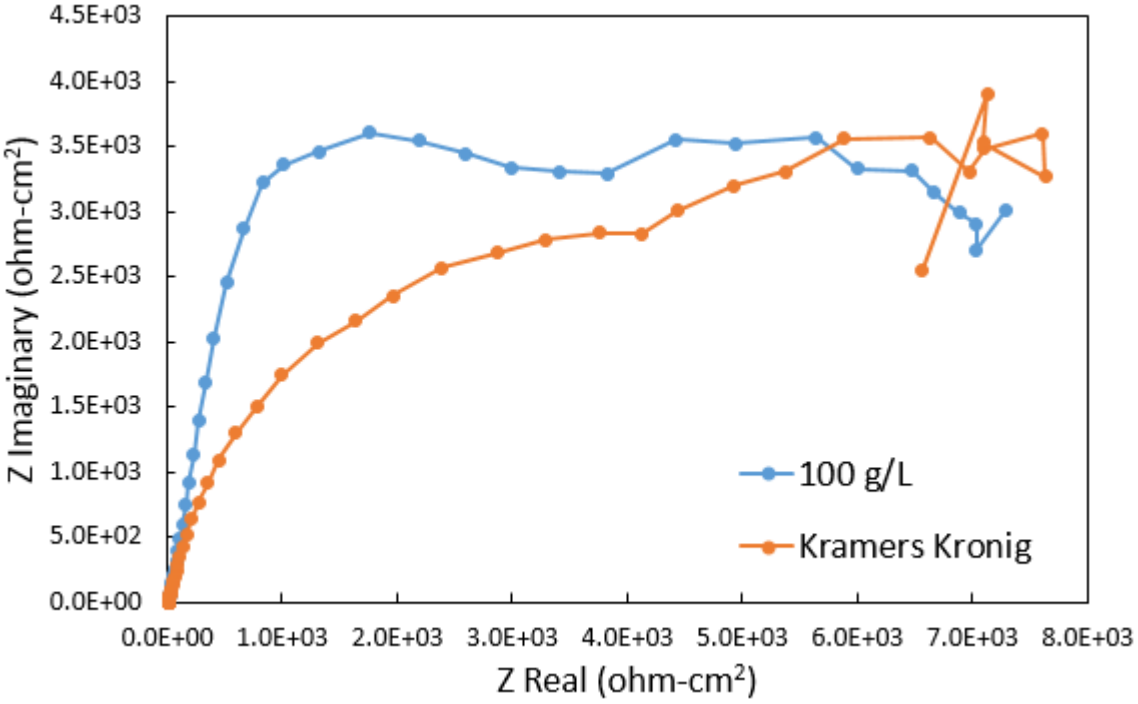

Figure 12. Kramers Kronig analysis on 100 g/L sample for EIS

4.2.2 Electrochemical Frequency Modulation

Operating in the non-capacitive region, the Tafel constant for each sample was determined. EFM also yielded the corrosion current. Both of these parameters can be seen in the figure below. A checkmark pattern is consistent with both values. A lower Tafel constant is indicative of a faster reaction, because it takes less overpotential to accelerate the corrosion reaction.

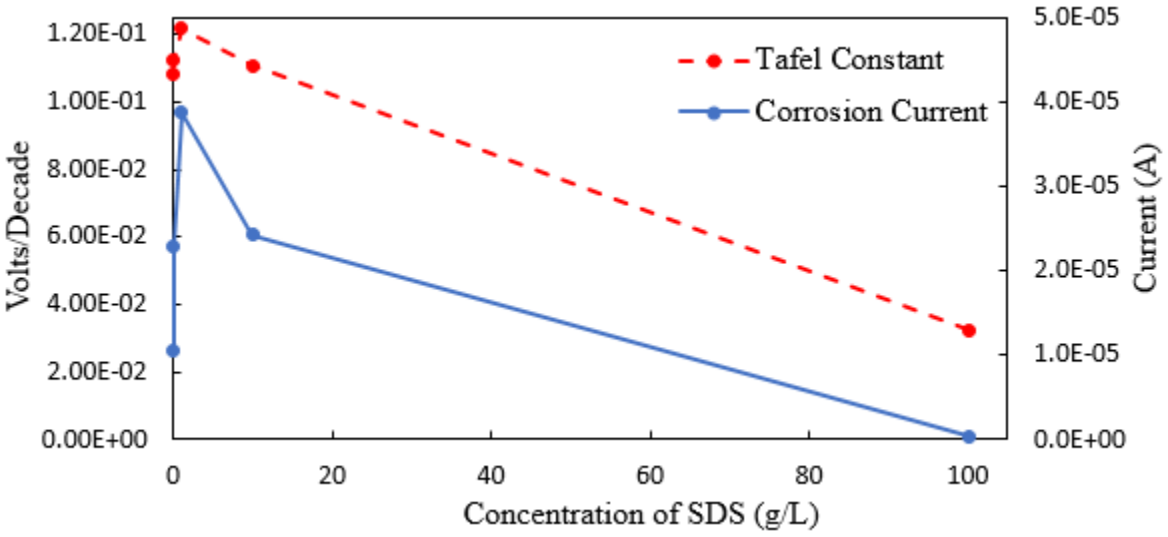

Figure 13. Tafel constant and corrosion current from EFM

The corrosion current peaks at 1 g/L SDS. This indicates that the most corrosion at OCP is occurring at this sample, while the least amount is occurring at the 100 g/L sample. This is an indication that corrosion is most thermodynamically favorable where it is slowest. Another way to explain this is that the 1g/L sample resists corroding, but once it starts corroding, it corrodes most quickly.

Causality factors 2 and 3 were measured for each run. These factors give insight into how much noise is detected during each experimental run. Ideally, causality factor 2 would equal 2, and causality factor 3 would equal 3. One experimental data point at 100 g/L was thrown out and retested because the causality factor 2 was approximately 687,000,000. It is unclear what caused this dramatic of a result. The most likely scenario is that the sample was acting as a capacitor, and this made the detected frequencies drastically different than expected. On average, causality factor 2 was found to be closer to ideal values than causality factor 3. The table below summarizes the causality factors for each concentration of SDS.

Table 3. Causality factors from EFM

SDS Concentration (g/L)	0	0.1	1	10	100
Causality Factor 2	1.81	2.05	1.99	1.99	1.62
Causality Factor 3	1.65	1.49	3.71	3.49	3.2

4.2.3 Galvanodynamic Scanning

Galvanodynamic scanning yielded curves for each sample showing the voltage versus the OCP against the normalized current. The Gamry packaged software was unable to process the data and perform a Tafel fit, but the comparisons between curves can still give insight. If these curves follow the same pattern of Tafel constants as calculated by EFM, it serves as an important confirmation of the observed trend. An accurate comparison between all of the curves cannot be achieved due to this error in the Gamry packaged software. Comparing the two extrema (1 g/L and 100 g/L SDS), as determined from other corrosion tests, could serve as a validity check for the other tests. The figure below depicts the results for the samples run at 1 and 100 g/L SDS.

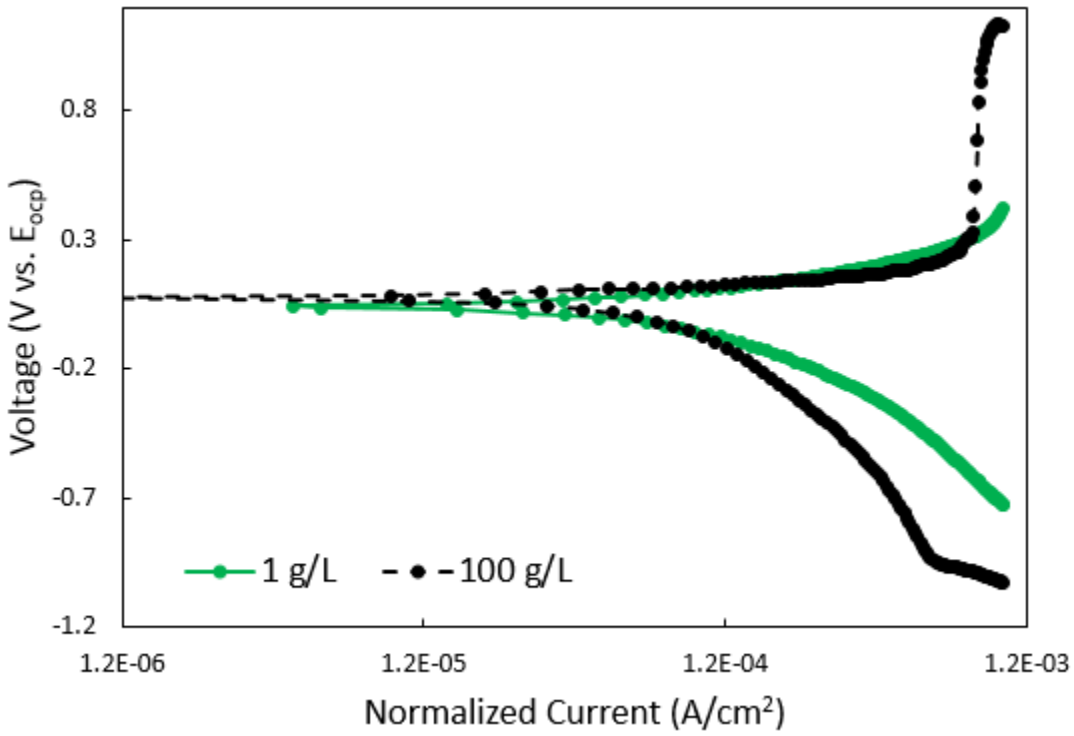

Figure 14. GDS results of samples produced at 1 and 100 g/L SDS

The graph can be divided into two halves: the negative voltage region and the positive voltage region. Corrosion occurring on the sample means that neutral metal is losing electrons to become metal cations, which then diffuse away. This means the sample is corroding in the positive voltage region. The large spike present in the 100 g/L sample would represent a passivation region, where negligible current density increases correspond to a large spike in the potential. While there are corrosion potentials for both curves, the 100 g/L sample also has a pitting potential (Shi et. al, 2017). The passivation layer is destroyed, which can be seen as the flat top after the large spike in the potential. This test provides additional support for the theory that a passivation layer exists for the 100 g/L sample.

The relative magnitude of the Tafel constants can be estimated from this graph as well. Note how, for the primarily linear section in the positive voltage region, the 1g/L starts at a lower

potential than the 100 g/L sample, and also ends at a higher potential than the 100 g/L sample. This indicates that the 1 g/L sample has a larger slope over the linear, reaction controlled section of the graph. Tafel constants are precisely these slopes; this graph serves as further evidence that the 1 g/L SDS sample had a larger Tafel constant than the 100 g/L sample.

Another important parameter to compare is the relative slopes of these samples. The polarization resistance is essentially the slope from the linear region on either side of the corrosion potential. A larger slope here would indicate a larger polarization resistance, because it reflects a sample less willing to accept charge on its surface. The 100 g/L sample has a relatively large slope towards the tail of the curve, in the diffusion limited region. This corresponds to a much higher polarization resistance than observed on any other sample, because this region in GDS has an incredibly large slope compared to the other samples.

4.2.4 Linear Polarization Resistance

LPR was run on all five samples. In order to analyze the data from these experiments, the Tafel constants must be known. These kinetic parameters are found in the equations to yield

thermodynamic properties such as R_p and E_{corr}. R_p is then used to determine another kinetic property: I_{corr}. The constants calculated from EFM were used for the following analysis.

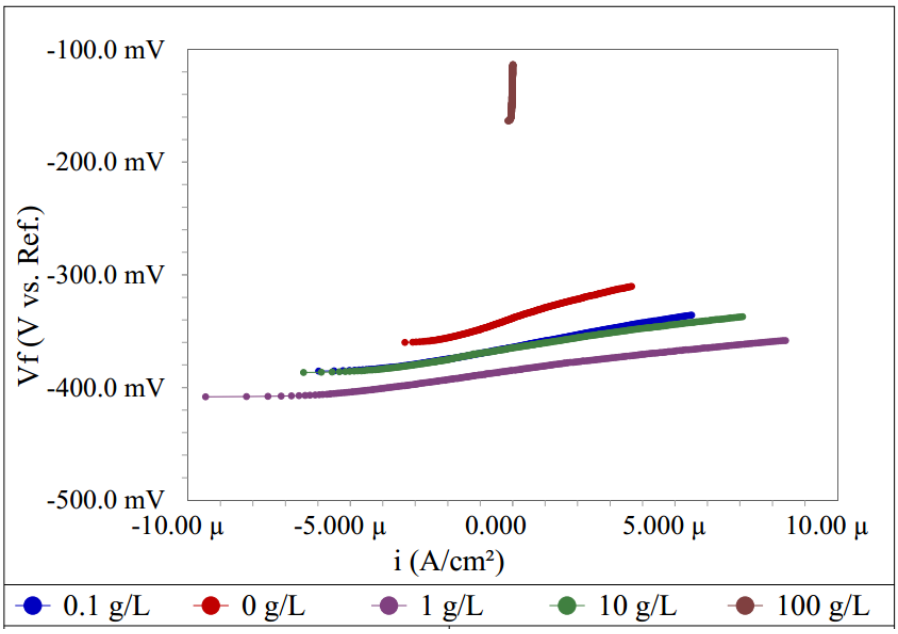

Figure 15. Results of LPR from each bath concentration of SDS

The figure above shows the results from LPR for films produced at each concentration of SDS. The slope of each line is the polarization resistance of that material; for example, the 100 g/L sample has the highest polarization resistance by far. The potential at zero current is E_{corr}, and serves as a measure of reactivity. The values of the corrosion potential will change depending on the environment in which corrosion occurs, but it still serves as a means of comparison between the samples. The data for corrosion potential and polarization resistance can be found in the figure below. Because LPR is calculated by taking the slope of the linear region surrounding a current density of zero, little error is associated with the R_p calculation itself. Only error propagated from the calculation of the Tafel constants (from EFM) would have significant effects on the following data points.

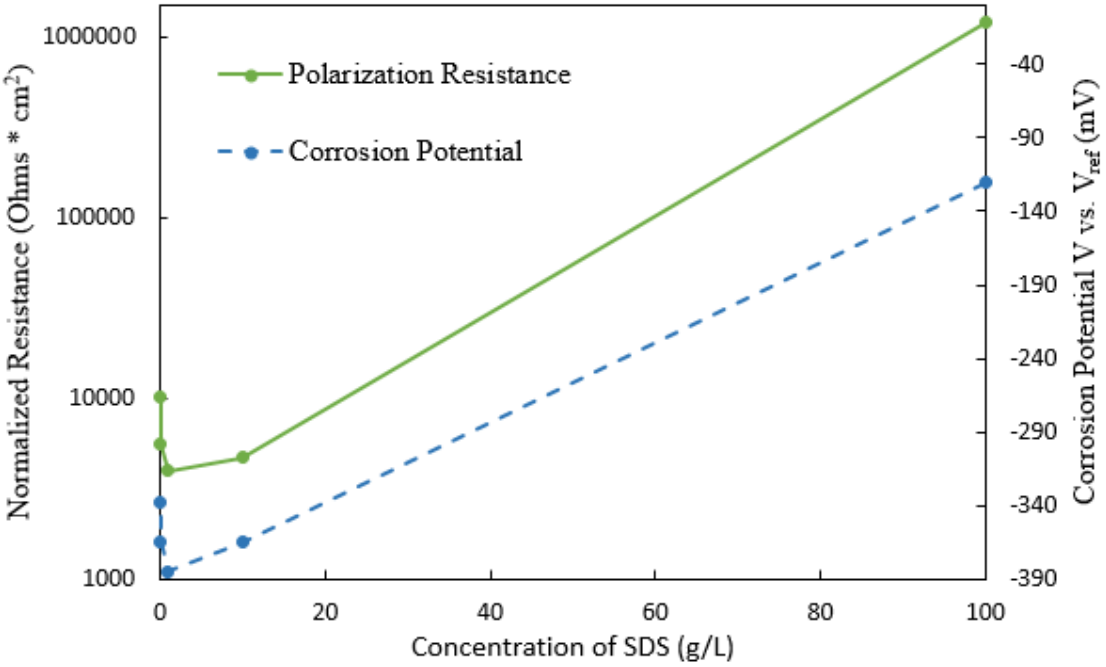

Figure 16. Polarization Resistance and Corrosion Potential from LPR

There is likely more than one factor influencing the polarization and corrosion potential as the concentration of SDS is varied. This would better explain the observed checkmark shape. The sample produced in 1 g/L SDS has the greatest tendency to corrode because it has the most negative corrosion potential. Samples produced in less and greater SDS concentrations all were thermodynamically less likely to corrode in a given environment. The sample least likely to corrode is the 100 g/L sample.

The final tabulated property was the corrosion current, and this was done by using a simplified version of the Stern-Geary equation in Gamry Echem Analyst. This equation utilizes both Tafel constants and the polarization resistance to determine I_{corr}. This property is directly proportional to the corrosion rate. The results can be seen in the figure below.

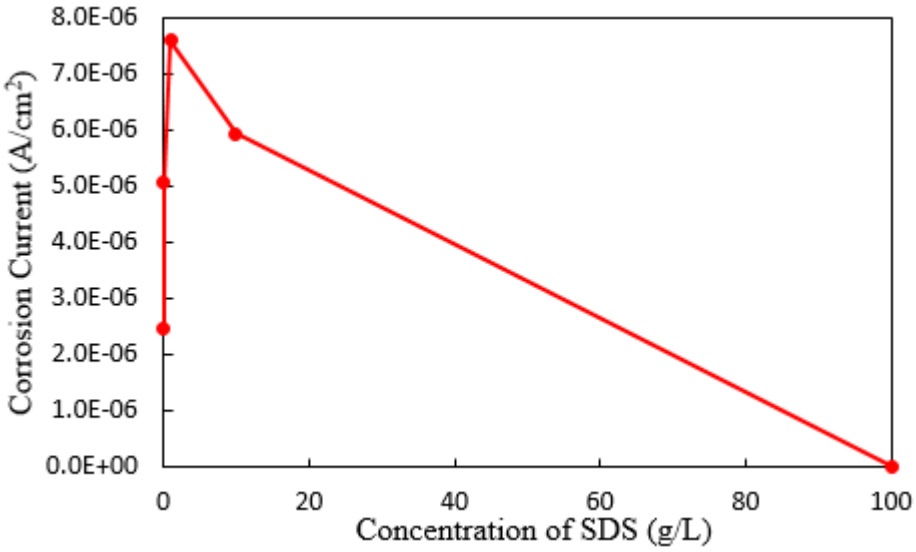

Figure 17. Corrosion current from LPR

Corrosion occurs quickest on the 100 g/L sample, and slowest on the 1 g/L sample. As also seen with the thermodynamic properties, a checkmark pattern is observed but here it is flipped vertically. This indicates that the film most resistant to initiating corrosion also will corrode the quickest once corrosion does begin.

Error analysis was conducted on how changes in the Tafel constants change polarization resistance, corrosion current and corrosion potential. The table below summarizes the results. It appears that R_p and E_{corr} work independently of the inputted Tafel constants. This makes sense because the corrosion current would be calculated after directly determining polarization resistance and corrosion potential from the slope of the collected data. The Butler-Volmer equation is used for this calculation; the Tafel constants are required for this equation, and therefore only I_{corr} is impacted by error propagated from Tafel constant determination.

Table 4. Dependence of LPR results on inputted Tafel constants

Changed:	**Resulting Changes in:**		
Tafel Constants	**R_p**	**I_{corr}**	**E_{corr}**
33%	0%	33%	0%
21%	0%	21%	0%
10%	0%	10%	0%
0%	0%	0%	0%
-10%	0%	-10%	0%
-19%	0%	-19%	0%
-27%	0%	-27%	0%

4.2.5 Summary of Corrosion Experiments

Most of the tests agreed in terms of the shape of the data. A checkmark pattern was observed for a majority of the tests, with the 1 and 100 g/L samples serving as the upper and lower extrema. EIS was the only exception, where the 100 g/L sample data appeared inaccurate after analysis using Kramers Kronig data fitting. This could indicate that instruments that are more precise are needed for EIS to be accurate, or that the 100 g/L sample was changing as the frequency was changed. This could be due to the disturbance of the passivation layer.

EFM proved an effective means of generating Tafel constants for samples without destroying them. The traditional method of getting Tafel constants, GDS, failed to produce enough linear sections to determine the Tafel constants. This could have been due to a diffusion-limited

system, rendering GDS useless. However, EFM can still obtain Tafel constants under these conditions while also being nondestructive.

Multiple tests indicate that thermodynamics and kinetics affect the corrosion rate antagonistically; as the thermodynamics become more favorable, the reaction proceeds slower. This type of behavior is documented in passivated systems. For example, chromium will resist corrosion in sulfuric acid at low temperatures, while iron will readily corrode. However, at higher temperatures, the passivation layer of Cr_2O_3 on the chromium film will be destroyed, and the sample will corrode even quicker than iron. It is possible that the dramatic increase in SDS concentration allowed SDS to adsorb on the surface and serve as a passivation layer. This made the material very resistant to corrosion, but when corrosion begins, it removes the passivation layer and may expose a more reactive film than those produced at lower SDS concentrations. This observation could also be the result of pitting corrosion caused by chlorine ions.

LPR showed unusual behavior relating to polarization resistance for the 100 g/L sample, and it was possible that the same sample previously had GDS run on it. This would explain why the curve is drastically different; the passivation layer was destroyed, so corrosion happened rapidly. This clearly demonstrates that nondestructive tests can be advantageous when many tests are desired. Using GDS or LPR could negatively impact the results of subsequent experiments, where EFM or EIS should not degrade the sample to any significant extent.

Chapter 5

Future Work

In order to compare samples made using different surfactant concentrations, certain assumptions had to be used. Future work in this area could focus upon proving the validity of these assumptions, as well as pinpointing the exact turning point in corrosion potential and Tafel constant values.

One of the key assumptions of this research is that SDS is not deposited on the surface in appreciable amounts. By directly comparing the results of LPS and EFM, this assumption helps isolate the difference of the depositions to be only by the spread of nanoparticles. This assumption could be tested by determining the Sulphur levels in each sample; even though saccharin deposits some Sulphur, the total amount should not be different at 0 and 100 g/L of SDS if the assumption is valid.

Going along with this, a constant composition was also assumed. That is, the percentage of iron, nickel, and alumina from sample to sample would have to be relatively constant for the results, as currently interpreted, to be correct. This applies to the composition of the solution, and this means that the same amount of nanoparticles was assumed to be deposited in each sample. Iron is known to be diffusion limited in these systems, so at very high SDS concentrations (>100 g/L) where the solution becomes exceedingly viscous the percentage of iron found in the film could decrease. Factors such as the stirring speed of the bath during deposition have a significant effect on the rate of iron deposition, so this assumption may not be valid. ICP-MS could be run to determine the validity of the conclusions of this experiment.

Another assumption was that ion loss from each run negligibly affected the overall concentration of ions. This allowed the experiment to be run sequentially with one bath. The result was using approximately 40 mL of bath instead of 240 mL. This could be verified by running one bath for many separate depositions and then determining if the composition changes as the number of runs increases.

The readily available reference electrode used for the corrosion experiments happened to have a relatively large amount of impedance. This meant impedance was added to the system, which could have affected the results. Repeating this experiment with a different reference electrode could test whether or not this added impedance had an effect on the experimental observations.

The critical micelle concentration for this solution is not known. At 100 g/L, the solution would at times become gelatinous. The thick foam would revert to the viscosity of approximately water after sonicating it for as little as 10 minutes at 20 ^{o}C. SDS forming micelles in the solution could have changed the bulk concentration of available nanoparticles or the mechanism of deposition. This could potentially invalidate the data point at 100 g/L, but also give insight into another potential way to control key properties of these nano-engineered surfaces.

Each of these factors or assumptions could affect how the results presented in Chapter 4 are interpreted. Future work should include investigating the concepts listed above and performing multiple experiments under the same condiions to test for repeatability.

Appendix A

List of Abbreviations

CPE – Constant phase element

E_{corr} – Corrosion potential

EFM – Electrochemical frequency modulation

EIS – Electrochemical impedance spectroscopy

GDS – Galvanodynamic scanning

I_{corr} – Corrosion current

ICP–MS – Inductively coupled plasma – mass spectrometry

LPS – Linear polarization resistance

OCP – Open circuit potential

OER – Oxygen evolution reaction

RE – Reference electrode

R_p – Polarization resistance

SDS – Sodium dodecyl sulfate

SEM–EDX – Scanning electron microscopy with energy dispersive X-ray spectroscopy

SS – Stainless steel

XRD – X-ray diffraction

Appendix B

In Depth Approach to EIS Modeling

Electrochemical impedance spectroscopy analysis works by taking the data collected and fitting it to an electrical circuit. The validity of the conclusions of EIS are only as valid as the model used; this Appendix is dedicated to the approach of determining and creating a viable equivalent circuit in order to calculate polarization resistance and solution resistance. This analysis of how to conduct EIS modeling is specifically tailored to the Gamry Electrochemistry Analyst software. The graph below shows the data that will be used for this guide, and it was the result of running EIS from 100000 to 0.005 Hz on a working electrode created with 0 g/L SDS. The Bode plot separates phase and magnitude of the impedance measurement. The curve made up of plus signs represent the phase of the measurement, while the curve made up of dots is the magnitude.

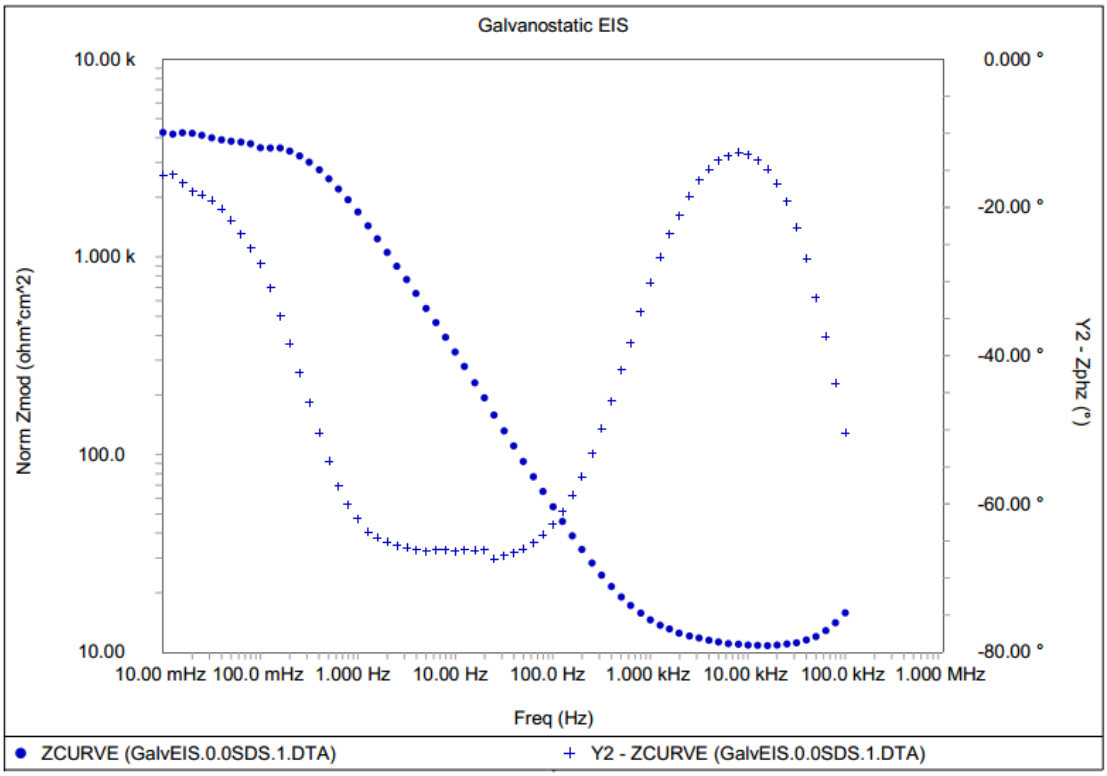

Figure 18. Raw data displayed in a Bode plot from EIS on a sample prepared in 0 g/L bath

Insight can be gained even without a model. For example, the non-capacitive region for the material can be determined by looking at the Bode plot. This region is essentially a range of frequencies where only negligible energy is stored by the system. This is a requirement for EFM, so conducting EIS first can allow a researcher to determine the settings at which to run EFM.

In order to determine the validity of the measured data, a Kramer-Kronig analysis will be conducted. It is a way take the real part of the measured data and calculate what the imaginary part should look like. This gives insight into how much feedback or inaccuracy is in the measurement. The goodness of fit was 0.077 for the data above, and it fits the Bode plot well. The displayed fit for the Nyquist plot shows some irregularities at the lowest frequencies, but this is expected because noise affects results significantly more as the frequency decreases.

Models should only have circuit elements that are justified by a physical phenomenon; adding infinite circuit elements will result in a perfect fit, but the results will be meaningless. Various models can be found online that model different physical observations. The model displayed below is conservative in the fact that it only has three distinct elements. The resistor connected to the reference electrode (RE) named Ru is meant to capture the resistance of the solution itself. This does not have anything to do with the polarization resistance; this component is accounted for in the Rp resistor. The other element in this model is called a constant phase element (CPE), and it is incorporated into the circuit to model an imperfect capacitor. This represents the physical phenomena of an electrical double layer.

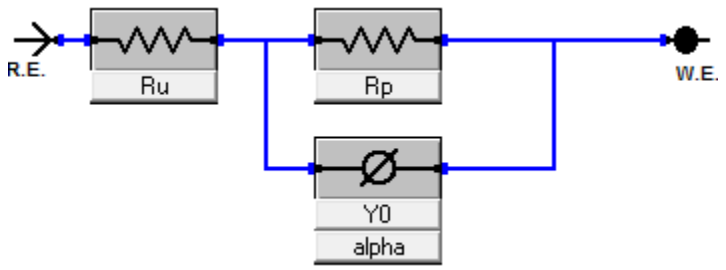

Figure 19. Equivalent circuit model without a diffusion element

Another option would be to include a circuit element that accounts for diffusion. If this model fits significantly better than a model without that element, it is likely that the system is diffusion limited or under mixed control. Typically, multiple elementary circuit elements would be necessary to create the effect that diffusion does; however, using one of three Warburg impedance elements allows diffusion to be accounted for easily. There are the infinite Warburg, bounded Warburg, and porous-bounded Warburg. According to the user guide for the Gamry Echem Analyst software, the infinite Warburg assumes an infinite and flat electrode where diffusion occurs perpendicular to the surface. The bounded Warburg element is most appropriate to use when there is only a thin layer of electrolyte surrounding a planar electrode. The porous Warburg is often reserved for systems similar to the bounded Warburg, but with the boundary of the electrolyte being a permeable membrane. The infinite Warburg is used in this experiment.

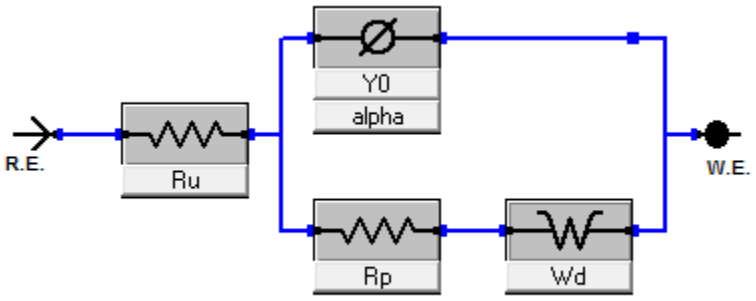

Figure 20. Equivalent circuit with an infinite Warburg element

The results of fitting both of these models using the Simplex method with a minimum of 300 points can be seen below. The goodness of fit for the model without diffusion elements and for the model with diffusion elements are 0.044 and 0.041 respectively. This difference is negligible and both fit the Bode plot

fairly well. This suggests that the corrosion occurring on the surface is not diffusion limited. This information is valuable because certain analyses such as GDS are only valid when there is no diffusion limitation in the system.

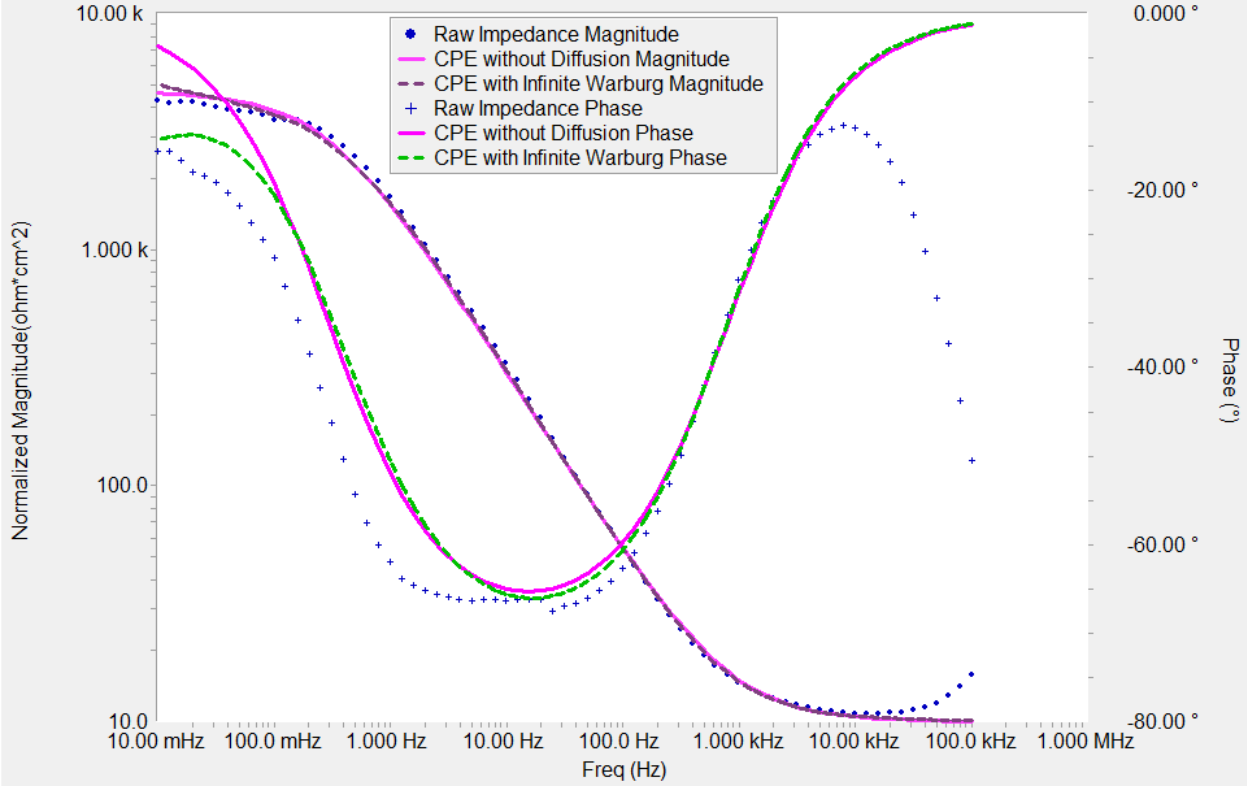

Figure 21. Bode plot with multiple model fits assuming different rate determining steps

The Nyquist plot, which contains both magnitude and phase in a single curve, is shown below for both types of models. If the model were truly diffusion limited, a curvature towards higher real component would be observed. This would mean there would be no expected contact with the x-axis. This has significant implications because polarization resistance is typically calculated by extrapolating the data after fitting it to a curve. The distance between the two parts of the curve that intersect the x-axis is the polarization resistance, while the distance between the y-axis and the closest x intercept graphically shows the solution resistance.

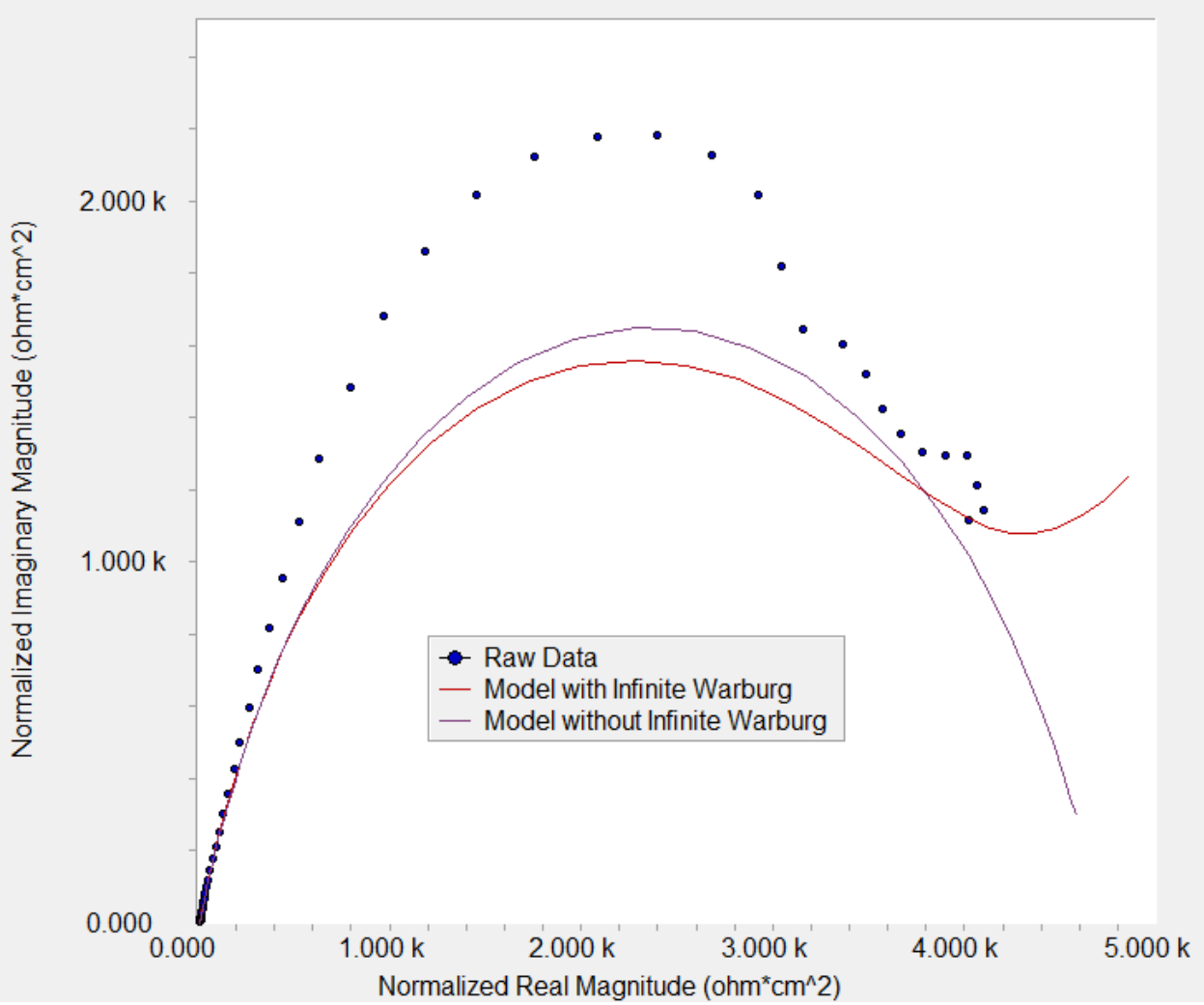

Figure 22. Nyquist plot with models assuming reaction and diffusion limited rates

To summarize, EIS scans a range of frequencies and determines what the impedance is at each point. Impedance consists of a magnitude and phase, and this data can be shown as separate curves in a Bode plot, or in one curve in a Nyquist plot. The Bode plot graphically shows the non-capacitive region and is useful for determining at what conditions to run EFM. The Nyquist plot graphically shows the rate controlled nature of the reaction, the solution resistance, and the polarization resistance. Insight into the latter two characteristics of the reaction is dependent on a good model. Models should only have components that can be described via physical processes, and are constructed as equivalent circuits in the Model Editor. This technique serves as a check to LPR, and helps determine how to run EFM.

BIBLIOGRAPHY

A. Bhandari, S.J. Hearne, B.W. Sheldon, S.K. Soni, Microstructural origins of saccharin-induced stress reduction in electrodeposited Ni, J. Electrochem. Soc. 156 (2009) D279-D282.

A. More, S. Bhavsar, G. Veser, Iron-nickel alloys for carbon dioxide activation by chemical looping dry reforming of methane, Energy Technol. 2016, 4, 1147.

D.V. Ribiero, C.A.C. Souza, J.C.C. Abrantes, Use of electrochemical impedance spectroscopy (EIS) to monitor the corrosion of reinforced concrete, Rev. IBRACON Estrut. Mater. 2015, 8, 4, 529-546.

H. Nakano, M. Matsuno, S. Oue, M. Yano, S. Kobayashi, H. Fukushima, Mechanism of Anomalous Type Electrodeposition of Fe-Ni Alloys from Sulfate Solutions, Mat. Trans. 45 (2004) 3130-3135.

J.R. Roos, J.P. Celis, J. Fransaer, C. Buelens, J. Met., 42 (11) (1990) 60

J. Wang, Z. Dong, J. Huang, J. Li, X. Jin, J. Niu, J. Sun, J. Jin, J. Ma, Filling carbon nanotubes with Ni-Fe alloys via methylbenzene-oriented constant current electrodeposition for hydrazine electrocatalysis, Appl. Surf. Sci. 270 (2013).

K.H. Kim, J.Y. Zheng, W. Shin, Y.S. Kang, Preparation of dendritic Ni-Fe films by electrodeposition for oxygen evolution, Rsc Adv. 2 (2012) 4759-4767.

M. Ghorbani, A. Dolati, A. Afshar, Electrodeposition of Ni-Fe alloys in the presence of complexing agents, Russ. J. Electrochem. 38 (2002) 1173-1177.

M. Vadivel, R. Ramesh Babu, M. Arivanandhan, K. Ramamurthi, Y. Hayakawa, Role of SDS surfactant concentrations on the structural, morphological, dielectric and magnetic properties of $CoFe_2O_4$ nanoparticles, RSC Adv. 5 (2015) 27060-27068.

Nickel Plating Handbook, Nickel Institute. (2017) 15.

R. Starosta, A. Zielinski, Effect of chemical composition on corrosion and wear behavior of the composite Ni-Fe-Al_2O_3 coatings, Journal of Materials Processing Technology. 157-158 (2004) 434-441

R.V. Williams. Electroplating and Metal Finishing, 19 (3) (1966), 92.

US Mint: Coin Production, United States Mint. (2017).

V. Torabinejad, A. Sabour Rouhaghdam, M. Aliofkhazraei, M.H. Allahyarzadeh, Electrodeposition of Ni-Fe and Ni-Fe-(nano Al_2O_3) multilayer coatings, Journal of Alloys and Compounds. 657 (2016) 526-536.

V. Torabinejad, M. Aliofkhazraei, S. Assareh, M. H. Allahyarzadeh, A Sabour Rouhaghdam, Electrodeposition of Ni-Fe alloys, composites, and nano coatings – a review, Journal of Alloys and Compounds. 691 (2017) 841-859.

Y. Shi, B. Yang, P.K. Liaw. Corrosion-resistant high entropy alloys: a review. Metals 2017, 7, 43.

Y. Wu, D. Chang, D. Kim, S.-C. Kwon, Influence of boric acid on the electrodepositing process and structures of Ni-W alloy coating, Surf. Coat. Technol. 173 (2003) 259-264.

ACADEMIC VITA

Education

The Pennsylvania State University **University Park, PA**
Schreyer Honors College *Graduation: May 2018*
Bachelor of Science in Chemical Engineering
- Chemical Engineering thesis: Effect of surfactant concentration on alumina nanoparticle-iron-nickel composites

Professional Work Experience

University of Arkansas **Fayetteville, AR**
NSF Funded Researcher *May 2017-August 2017*
- Studied the effects of surfactant concentration on corrosion resistance of alumina nanoparticle, iron, and nickel systems with the goal of creating better catalysts and longer-lasting materials
- Determined that corrosion parameters peak between 0.1 and 10 g/L
- Interviewed 4 corrosion experts at 3M and AxNano to determine market potential of this technology within membrane systems in batteries and neutralizing water contaminants
- Developed a technique that allows for the accurate characterization of electrodeposited films 200% thinner using ICP-MS

Research

Kumar Lab **University Park, PA**
Undergraduate Researcher *January 2017-May 2017*
- Received a fellowship in the area of "Materials Inspired by Biology" from the NSF
- Investigated the use of halo-rhodopsin KR2 with potential applications in water desalination plants
- Created uniform (100 nm) asymmetric vesicles to model the pumping capabilities of the protein
- Worked towards embedding the protein all facing one direction, to maximize net transport

Leadership Experience

The Pennsylvania State University **University Park, PA**
Resident Assistant for Schreyer *August 2017-May 2018*
- Oversaw a floor of 40 diverse students, including 3 international students, in the honors residence hall and hosted at least one community building event per week
- Defused tense situations involving topics such as roommate conflicts and intoxication charges
- Managed a non-alcoholic "Paint n' Sip" event that had over 75 attendees

Be The Match - Nonprofit Organization **University Park, PA**
Event Coordinator *January 2014-November 2017*
- Organized a bone marrow drive in my hometown that raised over $300
- Trained 20 people on specific talking points and logistics for events
- Continue to volunteer at various Be The Match events hosted on campus

The Pennsylvania State University **University Park, PA**
Learning Assistant for Organic Chemistry II *August 2016-December 2016*
- Led group oriented study sessions with up to 80 students
- Designed 10 problem sets to test key concepts for 220 students
- Explained complex theory in an understandable, relatable manner

Awards and Honors

- Graduating in 3 cumulative years
- Received the Evan Pugh Senior Award for being in the top 0.5% of the graduating class
- Received the McWhirter Undergraduate Scholarship (2017-2018) for Student Excellence
- Received the distinction of National AP Scholar for achieving a score of 4 or higher on all 9 exams